ELSEVIER

Polymer 41 (2000) 3029–3035

polymer

Shear-induced coalescence in polymer blends—simulations and rheo small angle light scattering

C. Börschig, B. Fries, W. Gronski*, C. Weis, Ch. Friedrich

Materials Research Center, University of Freiburg, D-79104 Freiburg, Germany

Received 2 March 1999; accepted 24 June 1999

Abstract

The kinetics of shear-induced coalescence of polystyrene(PS)/poly(methyl methacrylate) (PMMA) blends containing 1 and 5% PMMA were studied as a function of shear rate with rheo-SALS (small angle light scattering). The growth of the average particle size is shown to be a function of total strain independent of shear rate, the growth rate being controlled by the volume fraction of the dispersed phase. The experimental behavior is quantitatively described by the simulation of the evolution of particle size distribution on the basis of non-linear rate equations including hydrodynamic interactions.

Keywords: Shear; Coalescence; Polymer blends

1. Introduction

Recently there has been increasing interest in understanding the complex processes that take place during the processing of polymer blends [1–3]. These efforts are motivated by the technologically important question of how a desired final morphology can be achieved by the proper choice of material parameters (composition, viscosities, interfacial tension) and processing conditions (temperature, shear rates, overall energy input). For optimum mechanical and optical properties, fine-structured morphologies on a submicron scale are generally desired, as fine dispersions or co-continuous morphologies with a low volume fraction of one component. In experimental investigations changes of material parameters are correlated to the morphology of the samples which have been removed from the mixing device after a certain residence time [1–3]. Since modeling of the complex processes occurring in the complicated flow pattern inside a mixer or extruder are beyond present computational capacities, simpler approaches have generally been taken. Recently Milner has simulated the dynamics by which a particle size distribution reaches a steady state using a simple model of a polymer mixer [4]. In this model the polymer material passes randomly from a low shear region where only coalescence of particles occurs to a region of high shear where only breakup of particles takes place. Simple shear is assumed in the two regions. The time dependent concentrations of a discretized droplet size distribution is described by a system of non-linear rate equations in which the rate constants for breakup and coalescence are dependent on the lifetime of the droplets and the collision rate in the low shear region. Whereas the first parameter is estimated by the rotation speed and the geometry of the mixer the latter is given by the ballistic collision rate modified by hydrodynamic and repulsive interactions. Specifically, the repulsive effect of block copolymers acting as surfactants is treated in detail. Hydrodynamic interactions are introduced by the model of Wang et al. who have solved shear induced collision between two spherical droplets for different ratios of viscosities and droplet radii [5].

These theoretical studies stimulated our interest in measuring the kinetics of one of the relevant processes, coalescence, by small angle light scattering (SALS) under well-defined flow conditions in a rheometer. We then compared these results with simulations in order to test the underlying physical assumptions, in particular the effect of hydrodynamic interactions. SALS has been used previously to demonstrate the effect of block copolymers on shear-induced coalescence, however, without considering the kinetics of the process [6]. A detailed experimental and theoretical investigation of the kinetics of flow-driven coalescence appeared recently [7]. Unlike the present work, this study is based on a different theoretical model in which coalescence is governed by drainage of the fluid film

* Corresponding author. Fax: +49-761-6319.
E-mail address: gronski@uni-freiburg.de (W. Gronski).

0032-3861/00/$ - see front matter
PII: S0032-3861(99)00456-5

Table 1
Characterization of polymers

Polymer	M_n (kDa)	M_w/M_n	η_0 (kPa s)
PS	96.4	0.3	2.4
PMMA	40.0	0.19	10.0

between colliding particles [8], whereby hydrodynamic interactions and the evolution of the particle size distribution under flow are ignored.

2. Experimental

2.1. Methods

Shear induced coalescence was measured in a Bohlin stress rheometer in which a SALS-apparatus equipped with 2D detection by a CCD camera is integrated. The apparatus described elsewhere [9] was modified for use at high temperatures [10]. Experiments were carried out at 210°C. The use of a shear cell with cone angle 1° avoided air inclusion when closing the shear cell entirely. The thickness of the scattering volume was 200 μm. For transmission electron microscopy (TEM) ultrathin sections were obtained using a Leica Ultracut-E microtome. Elastic bright field images were taken on a Zeiss CEM 902 operating at 80 kV with monoenergetic electrons (ESI mode). Particle size distributions were analyzed using the image processing system SIS. The non-linear rate equations of the coalescence kinetics were integrated by a Runge Kutta routine using the software Matlab.

2.2. Materials and sample preparation

Blends were prepared from commercially available polystyrene (BASF) and poly(methyl methacrylate) synthesized by anionic polymerization. The analytical data of the polymers is given in Table 1. Blends containing 1 and 5 wt% PMMA were prepared by melt-blending 30 g of the mixture in a Randcastle Microextruder at 210°C. After extrusion the sample was melted under vacuum at 210°C. Pellets 40 mm in diameter and 0.2 mm thick were pressed in a hydraulic press for 5 min at 230°C and cooled to room temperature.

3. Simulation of shear induced coalescence

In the following, the kinetics of shear induced coalescence is described under the assumption of non-deforming spherical particles of radius r [5]. This is the case if the Weber number $We = \eta_m \dot{\gamma} r/\sigma$ is small or the relative viscosity $\eta_r = \eta_d/\eta_m$ is high, where η_m and η_d are the viscosities of the matrix and the dispersed phase, and $\dot{\gamma}$ and σ are the shear rate and the interfacial tension, respectively. It has been verified by light scattering that the assumption is fulfilled under the present conditions for shear rates $\dot{\gamma} < 1.0\ s^{-1}$. This implies that droplet breakup can be neglected, i.e. the development of the morphology is governed solely by coalescence.

If hydrodynamic and direct interparticle interactions are neglected the collision rate per unit volume in simple shear flow between particles of radii r_1 and r_2 (ballistic approximation) is given by [4]

$$J_{12}^0 = \frac{4}{3} n_1 n_2 \dot{\gamma} (r_1 + r_2)^3 \tag{1}$$

where n_1 and n_2 are the concentrations of particles with radius r_1 and r_2, respectively. In the presence of hydrodynamic interactions the rate of collision per unit volume is expressed by the ballistic collision rate times a collision efficiency $E(\lambda)$:

$$J_{12} = J_{12}^0 E(\lambda) \tag{2}$$

$E(\lambda)$ is a function of the radius ratio $\lambda = r_2/r_1$ ($r_2 \le r_1$ so that $\lambda \le 1$) that has been calculated numerically for different viscosity ratios $\eta_r = \eta_d/\eta_m$ of the dispersed and the matrix phase [5]. At high viscosity ratio the collision efficiency is greatly reduced. Further, $E(\lambda)$ decreases with the particle size ratio and vanishes at a certain critical λ_c. The critical size ratio decreases with increasing η_r. Therefore collisions are inhibited by hydrodynamic interactions for droplets of extremely different sizes. For the following simulation we adopt the numerical result for $\eta_r = 5$ given by Wang et al. [5] which is close to the experimental value of $\eta_r \approx 4$–5.

Following Milner's approach, the droplet size distribution is discretized in units of the smallest droplet volume $v_0 = (4/3)\pi r_0^3$ approximated by the average droplet size at the beginning of the experiment. Since the initial size distribution is quite narrow the approximation is not critical. Considering that a collision of a droplet of volume k with another droplet of volume l produces a droplet of volume $k + l$ a system of master equations of the droplet populations of the following form is derived

$$\frac{dP_n}{dt} = \sum_{k+l=n}^{N} C_{kl} P_k P_l - 2 \sum_{l}^{l+n=N} C_{nl} P_n P_l \qquad n = 1, 2, \ldots, N \tag{3}$$

where P_n is the concentration of droplets of size n. The first term represents the generation of droplets of size n and the second their disappearance by coalescence of a droplet of size n with a droplet of size l. For numerical reasons a maximal size N has to be assumed. The structure of the master equations is such that a broad transient size distribution is generated from the initial uniform distribution of size 1. After a sufficient period of time a stationary uniform distribution of droplets of maximal size N is obtained. From a physical point of view this is unrealistic because unlimited growth is expected if no breakup of the droplets occurs. The significance of the parameter N of the simulation will be

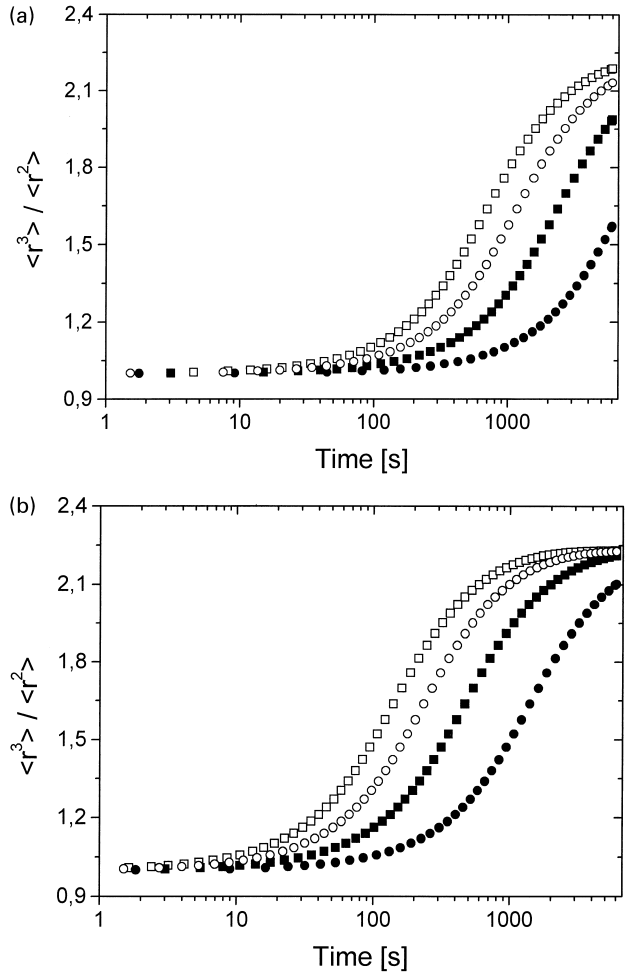

Fig. 1. Time development of the average droplet radius $\langle r^3\rangle/\langle r^2\rangle$ normalized to the initial radius for different shear rates (1.0 s^{-1} (□), 0.6 s^{-1} (○), 0.3 s^{-1} (■), 0.1 s^{-1} (●)), different volume fractions ϕ of the dispersed phase (ϕ = 0.01) (a), $\phi = 0.05$ (b)), and a cut-off parameter $N = 12$. Simulations with hydrodynamic interactions.

discussed below where simulations are compared to experiments. Eq. (3) fulfils the requirement that the total droplet concentration $P_0 = \sum nP_n$ or volume fraction $\phi = v_0P_0$ is conserved. According to Eq. (2) the collision kernels are defined by

$$C_{kl} = \frac{4}{3}\dot{\gamma}r_0^3(k^{1/3} + l^{1/3})^3E(\lambda) \tag{4}$$

when hydrodynamic interactions are considered or with $E(\lambda) = 1.0$ without hydrodynamic interactions. The master equations of (3) are solved for the time dependent populations by a Runge–Kutta Algorithm. For this it is convenient to introduce the reduced concentrations $x_n = (v_0/\phi)P_n$ which changes the collision kernel to $C'_{kl} = C_{kl}(\phi/v_0)$ showing that the rate at which the distribution changes is proportional to $\phi\dot{\gamma}$. For the simulations a uniform initial distribution has been assumed ($x_1(0) = 1.0$; $x_k(0) = 0$, $k > 1$).

The experimentally measured quantity is the correlation length that is proportional to the ratio of the third and second moment $\langle r^3\rangle/\langle r^2\rangle$ (see Eq. (6)). Fig. 1 shows the time development of $\langle r^3\rangle/\langle r^2\rangle$ normalized to the initial radius r_0 for various shear rates and two volume fractions that are realized in the experiments. The presence of hydrodynamic interactions with the efficiency function $E(\lambda)$ was assumed. The rate at which the particles grow by coalescence can be seen to increase with increasing shear rate and volume fraction. After a sufficient length of time a plateau value of $N^{1/3}$ is reached due to the limitation of droplet sizes.

Writing the master equations in dimensionless form by introducing x_n and the total strain $\gamma = \dot{\gamma}t$ as independent variables the reduced dimensionless collision kernel is $C'_{kl} = C_{kl}\phi/(\dot{\gamma}v_0)$. The rate at which the distribution changes as a function of strain is then independent of shear rate depending only on volume fraction. The simulation of the reduced value $\langle r^3\rangle/\langle r^2\rangle$ for two volume fractions is displayed in Fig. 2. The cut-off parameter N of the size distribution was also changed showing that the growth rate is not dependent upon N. By comparing the observable ratio $\langle r^3\rangle/\langle r^2\rangle$ with the number average $\langle r\rangle$ (Fig. 3), it can be seen that in the initial state the size distribution is uniform and both quantities coincide. With proceeding coalescence the particle size distribution broadens and the number average exhibits increasing negative deviation. When the strain (time) increases yet further, the deviation diminishes again because the size distribution narrows and eventually ends in the final state in which droplets are of uniform size. It must be noted that the narrowing of the distribution does not occur in reality, rather it is a consequence of the artificial limitation of the size distribution, which had to be introduced for computational reasons. In reality, the particle size is broadened and grows continuously as shown in the following paragraph. Fig. 3 also displays the simulations in

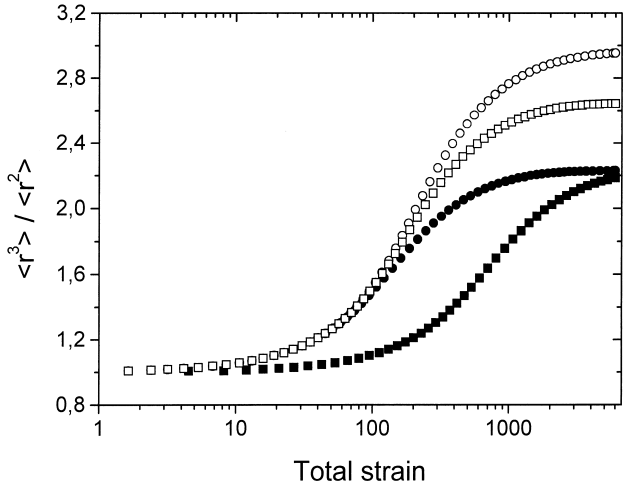

Fig. 2. Development of the average droplet radius $\langle r^3\rangle/\langle r^2\rangle$ normalized to the initial radius as a function of total strain at a volume fraction $\phi = 0.05$ for various cut-off parameters ($N = 28$ (○), $N = 20$ (□), $N = 12$ (●)). The lowest curve corresponds to $\phi = 0.01$ and $N = 12$ (■). Simulations with hydrodynamic interactions.

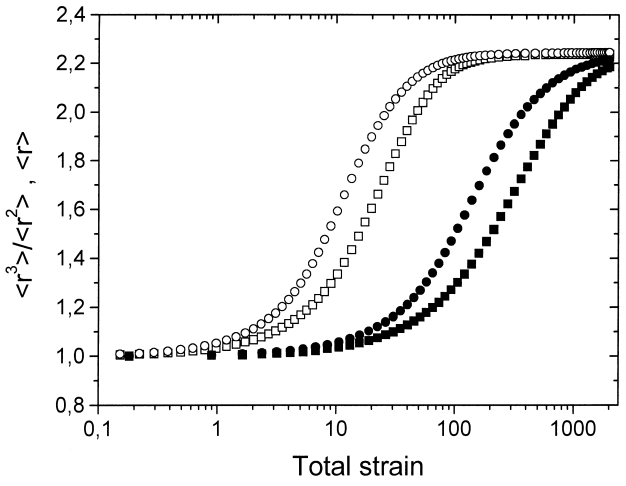

Fig. 3. Simulations with hydrodynamic interactions in comparison with the ballistic approximation: ballistic $\langle r^3\rangle/\langle r^2\rangle$ (○), ballistic $\langle r\rangle$ (□), hydr. int. $\langle r^3\rangle/\langle r^2\rangle$ (●), hydr. int. $\langle r\rangle$ (■). Volume fraction $\phi = 0.05$.

the ballistic approximation demonstrating that the rate of coalescence is significantly diminished by hydrodynamic interactions.

4. Direct observation by electron microscopy

Fig. 4 shows TEM micrographs of a 1% PMMA blend before shearing (a) and after shearing for an extended period (b). The number of particles is greatly reduced and the particle size distribution is broadened by shear-induced coalescence. The 2D diameters evaluated from TEM images are displayed in Fig. 5, quantitatively revealing the broadening of the size distribution. The initial size distribution was corrected for the thickness of the ultra microtome section by a regularization procedure [11]. The volume average radius of the corrected initial distribution $r_0 = 100$ nm has been taken as the initial uniform radius in the simulation of the experimental data.

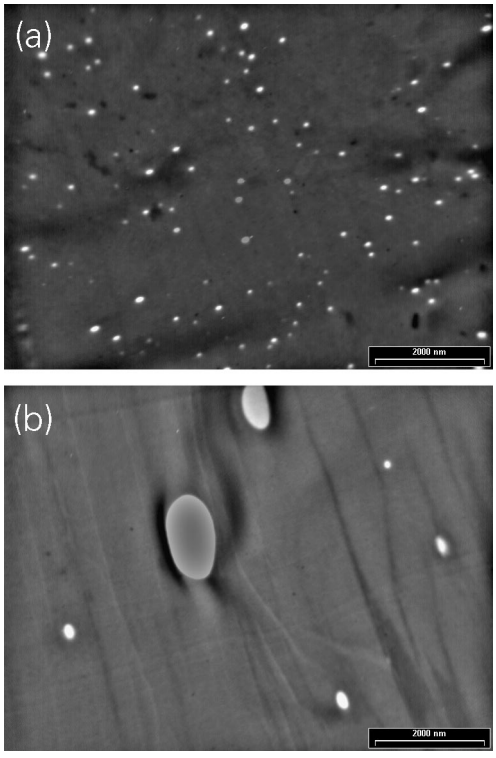

Fig. 4. TEM images of a blend with 1% PMMA (a) before shearing and (b) after shearing for 800 min at a shear rate $\dot{\gamma} = 0.02\ \mathrm{s}^{-1}$.

5. Light scattering

5.1. Data analysis

At low shear rates $\dot{\gamma} < 1\ \mathrm{s}^{-1}$ the scattering pattern remains isotropic at all times, i.e. the particles are not deformed. A typical development of the circular average of the intensity distribution is shown in Fig. 6 as a function of the scattering vector $q = (4\pi/\lambda)\sin(\theta/2)$. The intensity increases with time as a result of increasing droplet volumes. The scattering function was analyzed by the Debye Bueche scattering theory for statistical isotropic systems [12] according to the equation

$$I(q) = \frac{I(q=0)}{(1+q^2a_c^2)^2} \tag{5}$$

The correlation length a_c is inversely proportional to the specific surface S_{sp} of the scattering particles according to $a_c = 4\phi(1-\phi)/S_{sp}$ [12] and therefore is related to the second and third moments of the droplet size distribution by

$$a_c = \frac{4}{3}(1-\phi)\frac{\langle r^3\rangle}{\langle r^2\rangle} \tag{6}$$

The correlation length a_c is determined from the slope and intercept of a plot of $\sqrt{I}$ vs. q^2 [12]. The evaluation of a_c from the intensity distributions of Fig. 6 is displayed in Fig. 7. It can be seen that the average particle size as measured by a_c levels off after about 400 min although the droplets continue growing as documented by the intensity increase in Fig. 6 and also by TEM (Fig. 4). The effect is caused by multiple scattering that becomes more important with increasing particle volumes [13]. This leads to a smearing of the scattering distribution and limits the correlation length. This limitation has to be taken into account in the following evaluation and interpretation of the results.

5.2. Regime of small shear rates

We will first discuss the range of shear rates $\dot{\gamma} < 1\ \mathrm{s}^{-1}$. Fig. 8 shows that the correlation length or average particle size remains stable after cessation of shearing, begins to increase further after a second initiation of shearing and remains on the higher level after a second cessation. No relaxation effects are observed apart from some overshooting when the rotation of the cone is stopped. In Fig. 9 the

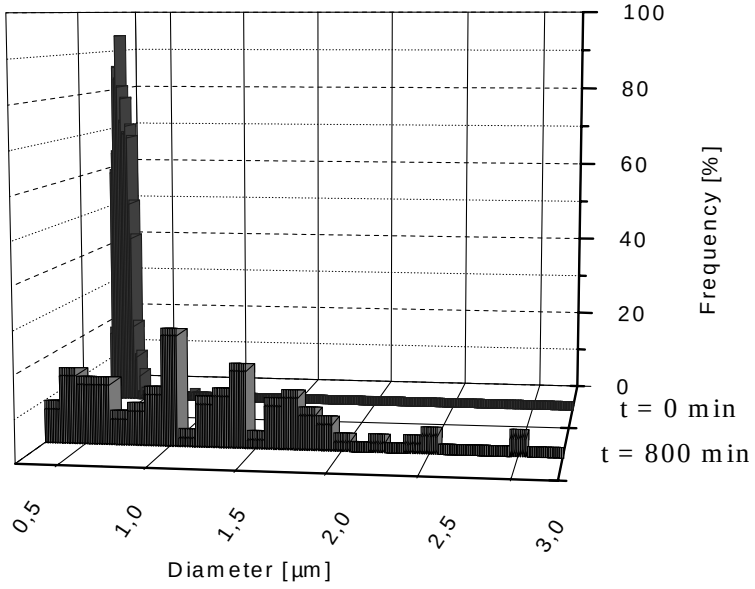

Fig. 5. Histograms of 2D diameters obtained from TEM images of a blend with 1% PMMA (a) before shearing and (b) after shearing for 800 min at a shear rate $\dot{\gamma} = 0.02\ s^{-1}$.

development of the correlation length is displayed for various shear rates and a volume fraction $\phi_{PMMA} = 0.05$. In the quiescent state ($t < 0$) the system is thermodynamically stable, and the average radius calculated from Eq. (6) is 100 nm assuming a uniform distribution. This value is in agreement with the average size of the corrected distribution determined by TEM. With the onset of shearing the correlation length (average droplet radius) begins to grow at a rate which increases with shear rate. If the data are displayed in dependence of total strain (Fig. 10) all data points fall on a common master curve independent of shear rate as suggested by Eq. (3) with γ as the independent variable. After sufficiently long shearing time or at high shear the correlation length reaches a plateau value. Since there are no breakup processes, which would stabilize a certain limiting particle size, the plateau cannot be a measure of the true size distribution. As shown by TEM the real size distribution is very broad. The average radius is in the µm-range, much larger than the apparent final size observed by light scattering. As explained above, this effect is caused by multiple light scattering, which limits the correlation length if the average particle volume exceeds a certain value. Since the apparent final radius is 2.2 times the initial radius of 100 nm, the maximum particle volume that is observed is about 12 times as large as the initial droplet volume at a volume fraction of about 5%. At a smaller total concentration the effect is expected to occur at a larger average particle size. Fig. 11, in which the data of experiments with blends containing 1% PMMA are shown, demonstrates that the plateau value of the correlation length is indeed somewhat larger compared to the blend with 5% PMMA.

The shape of the curves in Figs. 10 and 11 is similar to the shape of the curves which were simulated by the model for

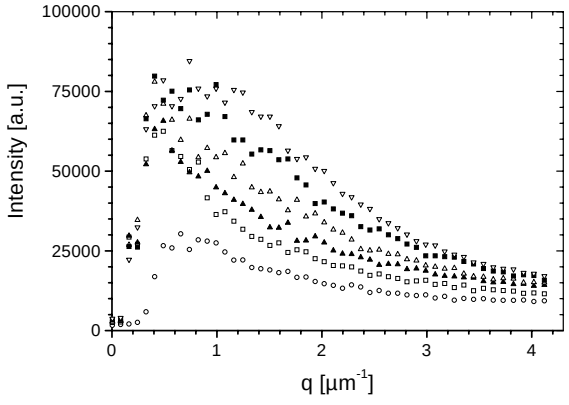

Fig. 6. Evolution of the scattering function recorded at different times after the onset of shear (0 min (○), 100 min (□), 200 min (▲), 400 min (△), 600 min (■), 800 min (▽)), $\dot{\gamma} = 0.02\ s^{-1}$, $\phi_{PMMA} = 0.5$.

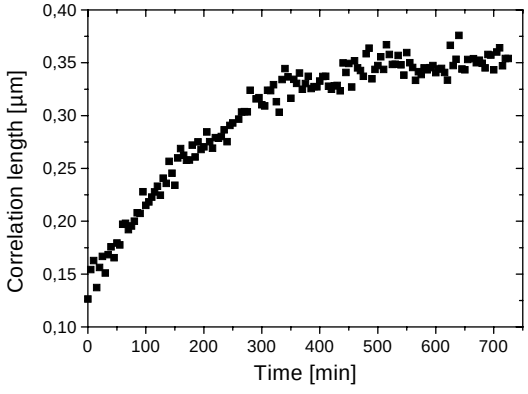

Fig. 7. Evolution of the correlation length during shear flow: $\dot{\gamma} = 0.01\ s^{-1}$, $\phi_{PMMA} = 0.05$.

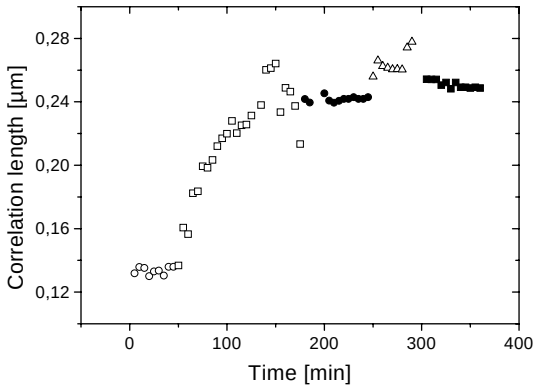

Fig. 8. Effect of intermittent shear: (quiescent conditions (○), first start of shear (□), first shear stop (●), second start of shear (△), second shear stop (■)), $\dot{\gamma} = 0.01\ s^{-1}$, $\phi_{PMMA} = 0.05$.

shear-induced coalescence according to Eq. (3). The cut-off volume N of the discretized particle size distribution can formally be identified with the maximum apparent particle size observed by light scattering. In fact, the experimental curves were simulated by the corresponding choice of $N = 36$ and $N = 12$ for the blends containing 1 and 5% PMMA, respectively. Besides the parameter N the only additional parameter in the strain dependent kinetics of the model is the volume fraction which determines the slope of the curves. The question is whether the presence of multiple scattering not only sets an upper limit to the observable particle size but also affects the observed growth rate of the droplets. This is not the case, because for the simulations of the master curves shown in Figs. 10 and 11 the volume fractions have not been treated as fitting parameters but have been set to the experimental values $\phi = 0.01$ and $\phi = 0.05$. Since the agreement with the experimental curves is excellent we conclude that the influence of multiple scattering does not falsify the determination of particle sizes at small strain values below the cut-off determined by multiple scattering effects. The simulated curves have been calculated assuming the presence of hydrodynamic

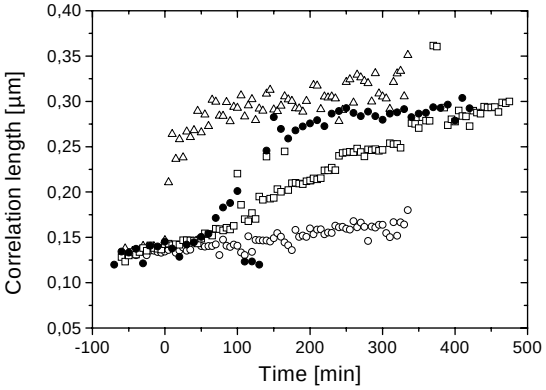

Fig. 9. Evolution of the correlation length at different shear rates as function of time ($0.0019\ s^{-1}$ (○), $0.036\ s^{-1}$ (□), $0.043\ s^{-1}$ (●), $0.47\ s^{-1}$ (△)), $\phi_{PMMA} = 0.05$.

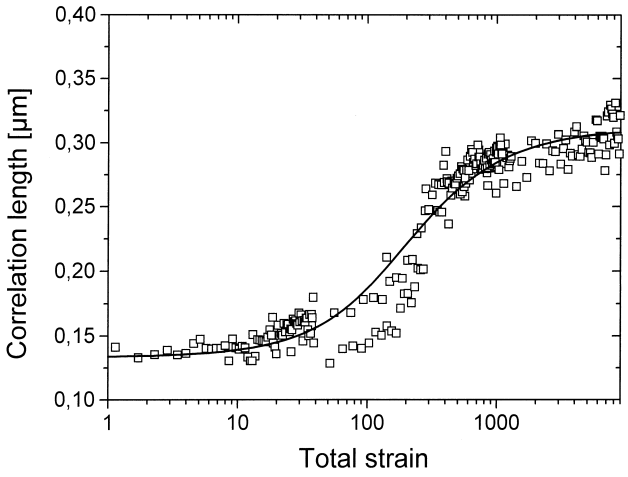

Fig. 10. Correlation length as a function of total strain. Shear rates and volume fraction as in Fig. 9 (experimental data (□), simulation with $\phi_{PMMA} = 0.05$ and $N = 12$ (—)).

interactions. Neglecting the interactions leads to a much faster growth rate as discussed in the theoretical section (Fig. 3). In the time dependent kinetics of Eq. (3) the growth rate additionally depends on the shear rate. In Fig. 12 the simulation is shown for a particular shear rate. The agreement between experiment and simulation is also satisfactory in this case.

5.3. Regime of high shear rates

In the range of shear rates $\dot{\gamma} > 1.0\ s^{-1}$ the scattering patterns are deformed to ellipsoidal patterns, the short axes of which point into the direction of flow, i.e. the droplets are elongated in the direction of flow. Two correlation lengths, one in the flow direction, the other in the neutral direction can be derived from the intensity distribution. A typical evolution of both correlation lengths is displayed in Fig. 13. At the onset of shear the correlation

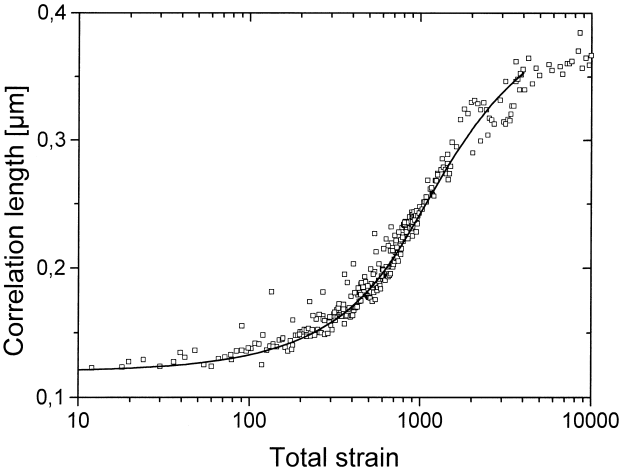

Fig. 11. Correlation length as a function of total strain at four different shear rates and $\phi_{PMMA} = 0.01$ (experimental data (□), simulation with $\phi = 0.01$ and $N = 36$ (—)).

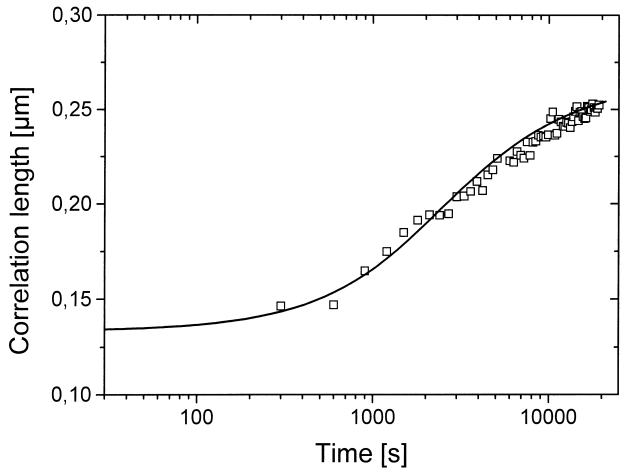

Fig. 12. Evolution of the correlation length as a function of time at $\dot{\gamma} = 0.75\ s^{-1}$ and $\phi_{PMMA} = 0.01$ (experimental data (□), simulation with $\phi = 0.01$, $\dot{\gamma} = 0.75\ s^{-1}$ and $N = 20$ (—)).

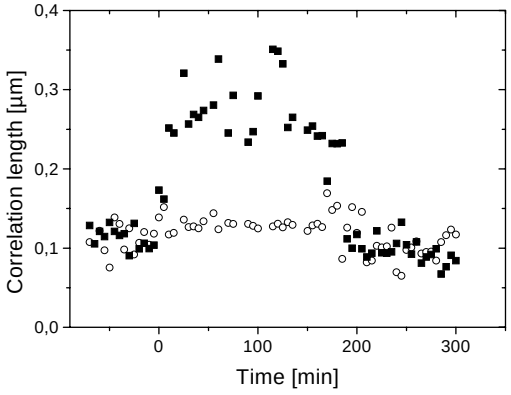

Fig. 13. Evolution of the correlation length at $\dot{\gamma} = 3.18\ s^{-1}$ and $\phi_{PMMA} = 0.05$ (direction of flow (■), neutral direction (○)).

length in the flow direction increases on the time scale of a few seconds, not resolved in the experiment. In contrast to the dimensions in the flow direction, the correlation lengths in the neutral direction remain constant with time. This seems to contradict the conservation of the particle volumes during deformation. A possible explanation for this behavior is that there is not only an upper limit of observable particle sizes caused by multiple scattering, but also a lower limit for a particle radius of about 100 nm as a consequence of the wavelength of light [14].

Fig. 13 further illustrates that the deformed droplets relax to their initial size and shape after cessation of shearing. From this observation we conclude that coalescence has not occurred to a significant degree, indicating that coalescence events are strongly reduced in case of elongated particles. The terms of the hydrodynamic interactions used in this coalescence model assume non-deformed droplets. Therefore, the effects we observed at higher shear rates cannot be simulated.

6. Conclusions

This is the first report on coalescence kinetics observed by rheo-SALS experiments for a typical polymer blend at high temperature. The measurements could be quantitatively analyzed within a limited observation window of particle sizes where the lower limit is determined by the wavelength of light and the upper limit by multiple scattering. It has been shown that hydrodynamic interactions strongly influence the coalescence kinetics. Thus, it was demonstrated that despite inherent limitations light scattering can be a powerful method to distinguish between different interaction models. In particular, the method should prove useful for direct measurement of particle growth during flow-driven coalescence when block copolymers are present as surfactants. This would verify or disprove, by direct measurement, the repulsion mechanism which has been postulated on the basis of mixing experiments [1–3] and a simplified model of the mixing process [4]. Investigations to this end are presently being carried out in our laboratory.

Acknowledgements

The work received financial support by the “Bundesministerium für Bildung und Forschung” through the “Arbeitsgemeinschaft für Industrielle Forschung” and by the SFB 428 of the “Deutsche Forschungsgemeinschaft”.

References

[1] Sundararaj U, Macosko CW. Macromolecules 1995;28:2647.
[2] Macosko CW, Guegan P, Khandpur AK, Nakayama A, Marechal P, Inoue T. Macromolecules 1996;29:5590.
[3] Beck Tan NC, Tai SK, Briber RM. Polymer 1996;37:3509.
[4] Milner ST, Xi H. J Rheol 1996;40:663.
[5] Wang H, Zinchenko AZ, Davis RH. J Fluid Mech 1994;265:161.
[6] Sondergaard K. Lyngaae-Jorgenson. J Polymer 1996;37:509.
[7] Vinckier I, Moldenaers P, Terracciano AM, Grizzuti N. AIChE J 1998;44:951.
[8] Chesters AK. Trans ICHemE 1991;69:A259.
[9] Läuger J, Gronski W. Rheol Acta 1995;34:70.
[10] Börschig C. PhD thesis, University of Freiburg. 1999.
[11] Friedrich C, Gleinser W, Korat E, Meier D, Weese J. J Appl Sci 1994;53:39.
[12] Stein RS. In: Paul DR, Newman S, editors. Polymer blends, 1. New York: Academic, 1978.
[13] Koberstein T, Stein RS. J Polym Sci Polym Phys Ed 1980;18:199.
[14] Stein RS, Srinivasarao M. J Polym Sci Polym Phys Ed 1993;31:2003.